SPACE TELESCOPE SCIENCE INSTITUTE
Operated for NASA by AURA

WFC3 Instrument Science Report 2015-16

Persistence in the WFC3 IR Detector: Spatial Variations

Knox S. Long, Sylvia M. Baggett, & John W. MacKenty
September 21, 2015

ABSTRACT

The amount of persistence observed in the WFC3 IR array varies slowly across the detector with more persistence in quadrant 1 than in quadrant 3. Variations in persistence are (mostly) not observed on small spatial scales. Here we describe attempts to quantify the nature of the persistence variations, and to incorporate a simple correction factor into the model for persistence in the WFC3 IR array.

Introduction

When images are obtained with the IR detector on WFC3, faint afterglows of earlier exposures are sometimes seen. The phenomenon is known as persistence, and is present to different degrees in all IR detectors. Persistence is due to traps in the diodes that constitute the pixels of an IR detector (See Smith et al. (2008ab) for a general discussion). The spatially-averaged characteristics of persistence in the detector in WFC3 have been summarized in a series of reports, most recently by Long et al. (2015). Persistence depends on the entire exposure history of a pixel; Long et al. (2015) parameterize this in a model based on the fluence (number of electrons accumulated) in an earlier exposure, the length of the exposure, and the time since the exposure.

Since we understand persistence as a trapping phenomenon, it is not surprising that persistence would vary across the face of the detector. This report summarizes some aspects of these variations and how we have used calibration files to create a "persistence flat" that partially accounts for these variations. In characterizing these variations, we make use the spatially-averaged model for persistence described by Long et al. (2015).

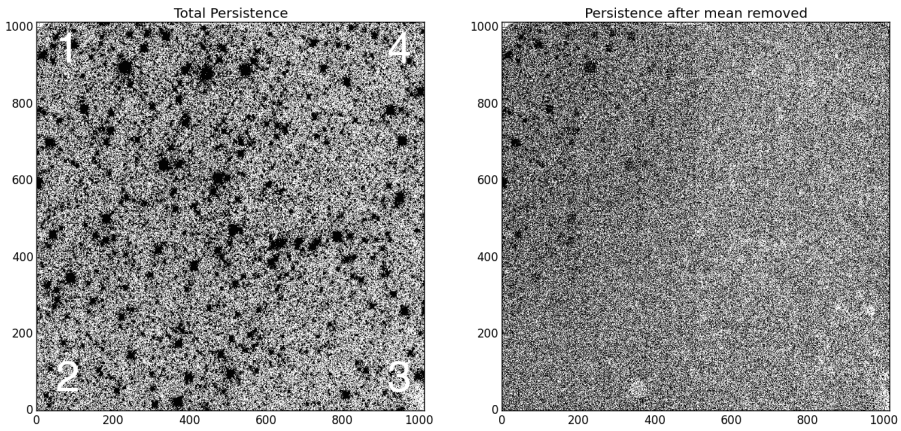

Figure 1. Left: Persistence observed in exposure icgk08e4q, a 352 s dark obtained approximately 400 s after the end of a 1400 s exposure of a portion of Omega Cen through the F547M filter as part of visit 8 of program 13572. The quadrant numbers are also shown. Right: Residual persistence after the mean persistence has been removed. Both images are linearly scaled from -0.005-0.005 e s^{-1} to emphasize regions where there is persistence. The mean persistence model underestimates the persistence in the upper left (quadrant 1) and overestimates it in the lower right (quadrant 3).

The nature of persistence in the WFC3 detector

There are two main types of calibration observations that have been carried out to characterize persistence in the IR detector of WFC3. The first involves observations of a relatively crowded star field, typically a region of Omega Cen or 47 Tuc, followed by a series of darks from which persistence is measured. The second involves an initial exposure with the tungsten lamp followed again by a series of darks. The advantages of the first type of calibrations are that these observations (a) start with a normal exposure, (b) result in a variety of fluence levels in a single observation, and (c) allow a more accurate measurement of the (variable) dark level since the star field exposure leaves some regions of detector at a low fluence level.[1] The advantages of the second type of calibration are that these calibrations do not require any external orbits and they expose all of the detector to a similar (but not completely uniform) fluence level. The two types of calibration provide somewhat different information about the nature of spatial variations in persistence.

The left panel of Fig. 1 shows a flux calibrated image of a dark exposure obtained about 400 seconds after a long exposure of a field in Omega Cen. Fluence levels in the initial exposure ranged from near 0 to well over 10^7 e, more than 100 times saturation.

[1]Fluence is defined to mean the total number of photo-electrons that result from the exposure.

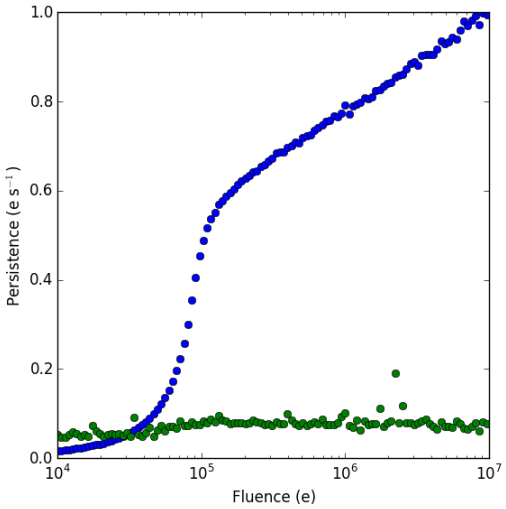

Figure 2. The average persistence (in blue) measured in the dark exposure icgk08e4q. The curve was obtained by binning groups of pixels with different fluence levels in the earlier Omega Cen exposure and taking the median value in each bin. The standard deviation about the mean is shown in green. At 10^7 e, the persistence in this image is about 1 e s^{-1}.

The average persistence in this (and in any dark) can be constructed from this image simply by binning up (averaging) all of the pixels in the dark which had a given fluence in the Omega Cen image. Results for this particular data set are presented in Fig. 2. The advantage of this approach is that it is essentially model-independent. The right panel of Fig. 1 shows the persistence with the average persistence subtracted. The figure indicates that persistence is more prominent than the average in the upper left hand corner (quadrant 1) and less prominent in the lower right hand quadrant (quadrant 3).[2] Persistence in the image peaks at about 1 e s^{-1}; the variation in persistence peaks at about $\pm$0.1 e s^{-1}. The general characteristics of the spatial variations are apparent in all observations of this type and do not appear to depend on factors such as the time since the external exposure.

The same type of analysis can be carried out for darks obtained after a tungsten lamp exposure. A typical example is shown in Fig. 3. In this particular case, the fluence in the tungsten exposure was about 10 times saturation and the dark was obtained about 1100 s after the end of the tungsten lamp exposure. As was the case in the example involving an external target, persistence is highest in quadrant 1, and decreases gradually across the the face of the detector. Some features, such as the "wagon wheel" in quadrant three are evident. The same features appear in the panel containing the image after

[2]We use the standard terminology for quadrants, where quadrants 1, 2, 3, and 4 correspond to the upper left (high row, low column) , lower left (low row, low column), lower right (low row, high column), upper right (high row, high column) quadrants, respectively. See Fig. 1.

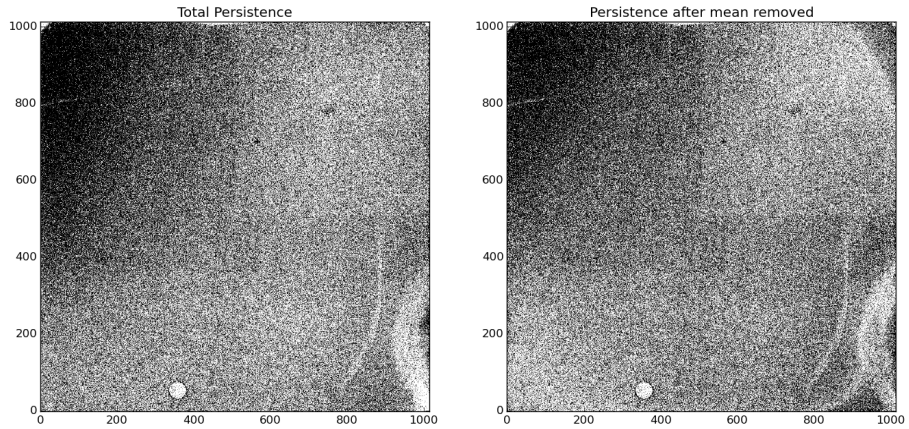

Figure 3. Identical to Fig. 1 but for the dark exposure ibmfabz6q. The persistence in this image was generated from a tungsten lamp exposure through the F105W filter lasting 1003 s. The mean fluence was about 700,000 e, or 10 times saturation. This particular dark was a 353 s exposure which began about 1100 s after the end of the tungsten lamp exposure. The mean count rate in the dark, which is almost entirely due to persistence, is 0.35 e s^{-1}. The flux in the quadrant 1 rises to about 0.45 e s^{-1}.

subtracting the average persistence, using the values displayed (in blue) in Fig. 4. A smoothed version of the residual persistence is shown in Fig. 5. There are small regions of the detector that appear to show enhanced persistence compared to the surrounding regions, several "features" at the corners of of the detector, and some slight differences in quadrants that are evident.

The tungsten lamp does not illuminate the detector completely uniformly, and therefore one might worry that this somehow accounts for the large scale variations that we see. A representation of the flt file associated with dataset ibmfabyxq, the tungsten lamp exposure which generated the persistence in Fig. 3, is shown in Fig. 6.[3] The processed image indicates that the the lamp illuminates quadrant 3 more than quadrant 1 thus the variations in persistence that we see in Fig. 3 are not due to differences in illumination. In fact, quite the opposite: since persistence increases with fluence we would have expected more persistence in quadrant 4 than quadrant 1, were it not for spatial variation in the persistence properties of the detector.

[3]To obtain the flt image with the gain correction applied, we processed the data as one would a normal external exposure, except that we used a "unity pflat", one in which all the values were set to one.

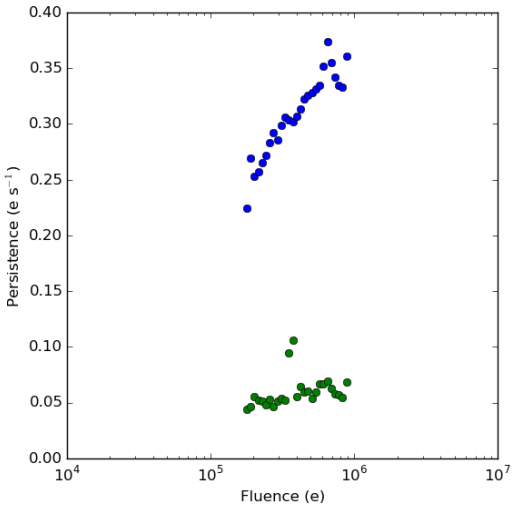

Figure 4. The average persistence (in blue) in the dark exposure ibmfabz6q, taken immediately after a tungsten flatfield exposure. The format of the figure is identical to that of Fig. 2.

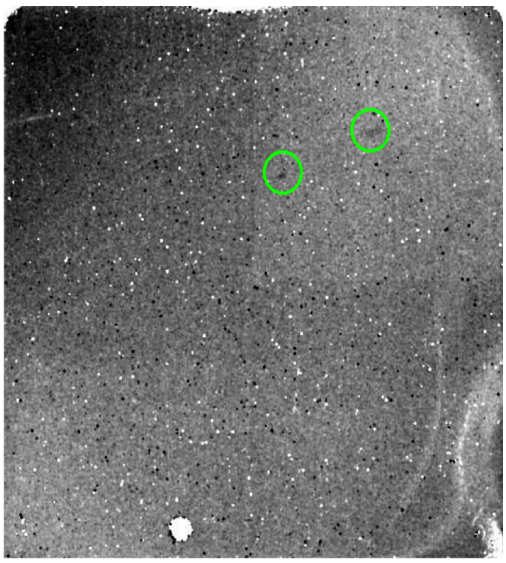

Figure 5. A smoothed version of the residual persistence measured in the dark exposure ibmfabz6q. Most of the very small scale structure in this images are due to individual pixels with poor data quality or cosmic rays, but there are a few regions, including those highlighted by the green circles, which appear to have excess persistence.

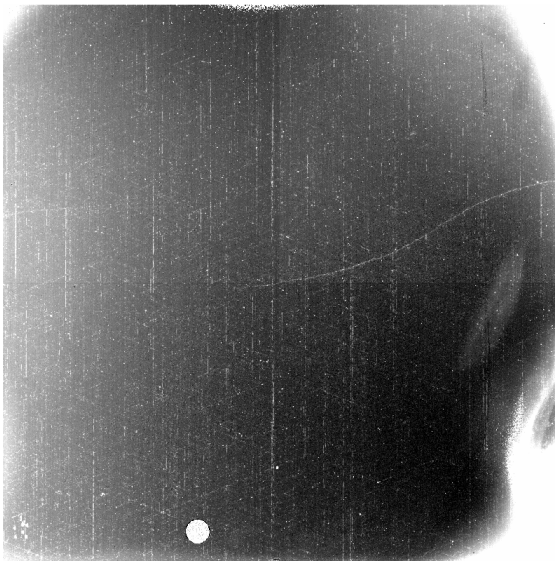

Figure 6. The tungsten image processed with a unity pflat and shown with an inverted greyscale. Count rates are highest in quadrant 3, of order 800 e s^{-1}, compared to 680 e s^{-1} in quadrant 1.

Quadrant by quadrant variations in persistence

We do not have enough calibration data to analyze persistence on a pixel by pixel basis. However, we can use the data from program 13572, which Long et al. (2015) use to create a model of spatially averaged persistence, and analyze data in subsections of the detector. In that report, Long et al. describe persistence in terms of a power law of the form:

$$P = A \left(\frac{t}{1000\ s} \right)^{-\gamma} \tag{1}$$

where A represents the amplitude of the persistence at 1000 s as a function of the fluence (measured in electrons) of an earlier exposure, t is the time since the end of the earlier exposure, and γ is the power law exponent, which is also a function of the fluence.

To carry out an initial characterization of how persistence varies across the detector, we have simply fit the data from each quadrant separately. The results are shown in Fig. 7, based on two observations of Omega Can with initial exposure times of 799 and 1102 s.[4] To zeroth order, the properties of the 4 quadrants are fairly similar. All quadrants have very little persistence when sources are below about 30,000 e; the persistence in all quadrants rises significantly in regions with saturated sources (70,000 e), and the shape of the amplitude curve has about the same slope in all quadrants. The power law

[4]We have avoided using visits where 47 Tuc was the stimulus image, because stars in that image are not spread uniformly across the detector.

decay exponents are also similar, higher at low fluence levels than at high fluences and leveling out at an exponent of just less than 1 above a saturation level around 10^5 e. The main difference is that the amplitude of the persistence is higher in quadrant 1 than in the other quadrants. There also appears to be a small difference in the shape of the power law exponents. In particular, the slope of the persistence in quadrant 3 appears to be slightly less than that of the other 3 quadrants at very low fluence levels, and slightly higher between 30,000 and 100,000 e.

A question worth asking is suppose the power law index does vary from place to place, how much difference does this make in the calculated persistence. Suppose, for example, for a given fluence level, the average γ is 1, but in a particular region of the detector it is 0.9. Then assuming we have already corrected for amplitude variations as a function of position (implying that we have an accurate correction of the persistence there) then at 2000 seconds, the error in persistence will be 7% and at 5000 s, it will be 17%.

The persistence flat

We have suggested above that to first approximation the variations in persistence are primarily variations in the amplitude of persistence. If this is correct, then it is possible to construct a "persistence flat" $R(x, y)$ that captures this amplitude variation in terms of a departure from the mean persistence, such that

$$P(x, y) = R(x, y)P_{ave} \tag{2}$$

where P_{ave} is the spatially-averaged persistence model (which is a function of the fluence in the stimulus exposure, the time since the stimulus exposure, and the exposure time of the stimulus exposure [See, Equation 2 of Long et al. 2015]).

Given a sequence of darks containing persistence obtained after tungsten exposures, we can estimate $R(x, y)$,

$$R(x, y) = \frac{\Sigma w_i (P_i(x, y) - P_{ave})}{\Sigma w_i} \tag{3}$$

where $P_i(x, y)$ is the observed persistence in the a dark exposure, and w_i is some appropriate set of weights that accounts for the fact that persistence is difficult to measure at low persistence levels. Our approach has been to use P_{ave} as the weighting factor (since it is more difficult to estimate spatial variations in persistence when the persistence itself is small).

To create a correction flat, we have made use of a collection of persistence calibration visits involving tungsten lamp exposures followed by a series of darks obtained as part of programs 12089 and 12351. Before constructing the correction flat, we culled the visits to eliminate those with obvious anomalies (usually evidence of persistence from an exposure prior to the tungsten visits). The 47 visits that remain have tungsten lamp exposures that range from 32 to 2500 s, and these exposures were obtained through a

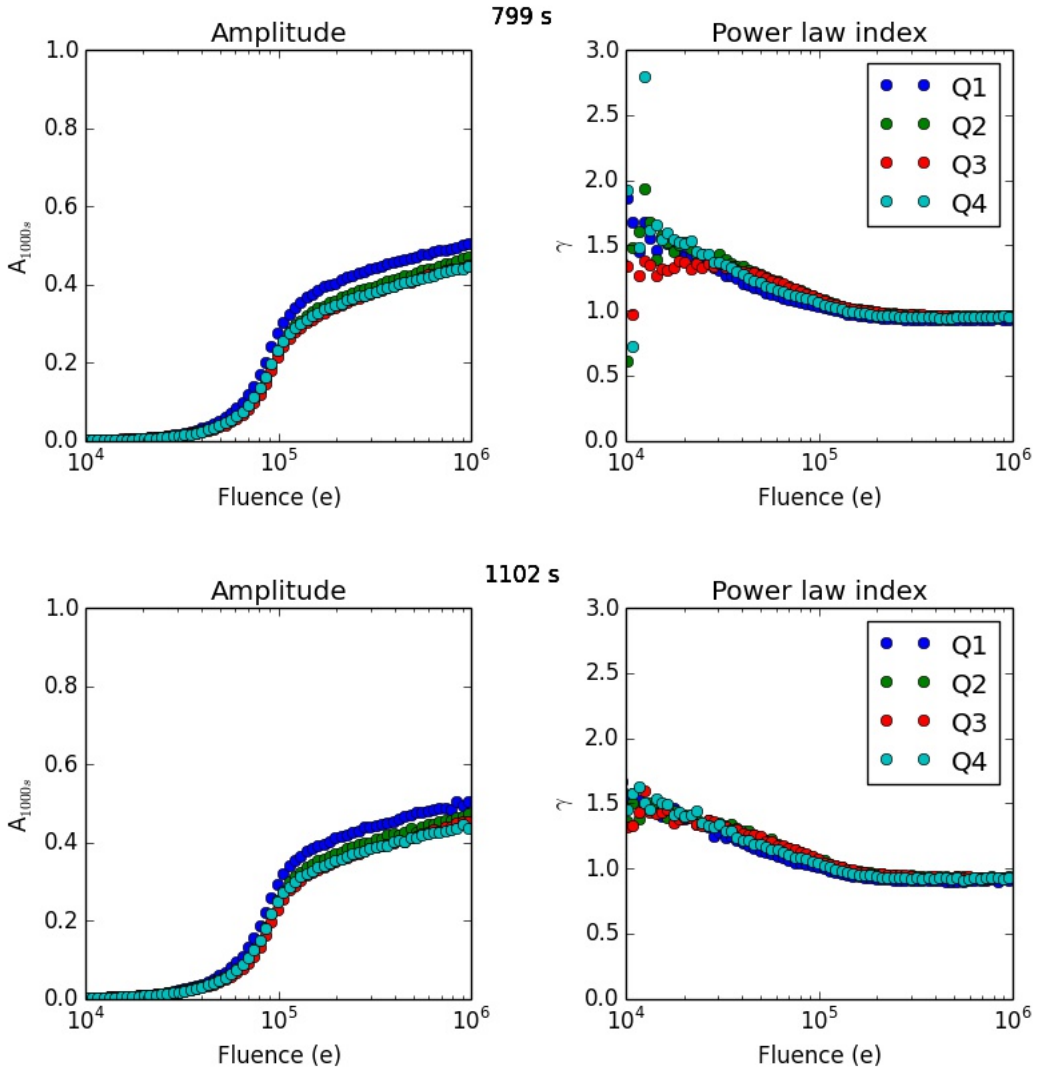

Figure 7. Calculated amplitudes (A) and power law exponents (γ) for two visits in program 13572 consisting of a single exposure of a field in Omega Cen followed by a series of darks. The upper panels are for a visit in which the initial external exposure was 799 s in duration; the bottom panels are for a visit with an initial external exposure of 1102 s. At low fluence levels, below 30,000 e, the persistence and its decay with time are more difficult to measure, and this causes scatter in the power law index, evident especially in the upper right panel.

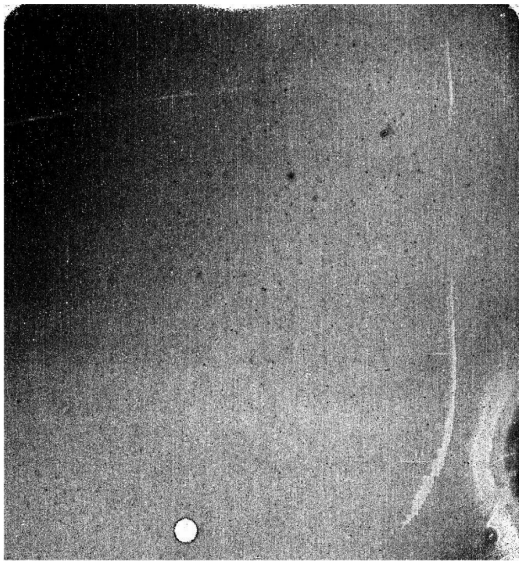

Figure 8. The correction flat derived from 47 visits, each involving a tungsten lamp exposure followed by a series of darks. The image is scaled from 0.8 to 1.2. The values of the correction flat are largest in quadrant 1 and lowest in various detector flaws, including the wagon-wheel feature.

variety of narrow, medium and broad band filters. As a result, they contain visits with a fairly wide range of saturation levels in the tungsten lamp exposures. However, it is important to recognize that these data do not represent a sample designed specifically for the purpose of creating the optimal correction flat.

We constructed the correction flat from 47 visits. We used data from a pixel in the correction flat if the spatially-averaged prediction for persistence was between 0.05 and 1 e s^{-1}. We constrained the values in the correction flat to be between 0.5 and 1.5.

The resulting correction flat is shown in Fig. 8. As expected, the correction flat resembles images obtained of the residual persistence produced in darks after tungsten lamp exposures, one of which was shown in Fig. 5. Values of the persistence correction flat in the corner of quadrant 1 are typically 1.4. The values of the correction flat in most of the other quadrants are close to or slightly less than 1, except for the flaws, the wagon-wheel and other scratches which have low values. There are a few regions, particularly, in quadrant 4, which are "splotches" of high persistence.

As noted earlier, we have used a rather heterogeneous set of data obtained for a variety of purpose to generate the persistence flat shown in Fig. 8. An interesting question therefore is the degree to which the correction flat varies depending on the data used to generate the flat. There are a variety of possible variations that one might want to investigate. There may be variations in persistence in nominally identical exposure sequences, which if spatially dependent would cause differences in the correction flat. Despite our assertion that to first order, spatial variations in persistence are amplitude, and delay-time related, persistence could decay away more rapidly in some sections of

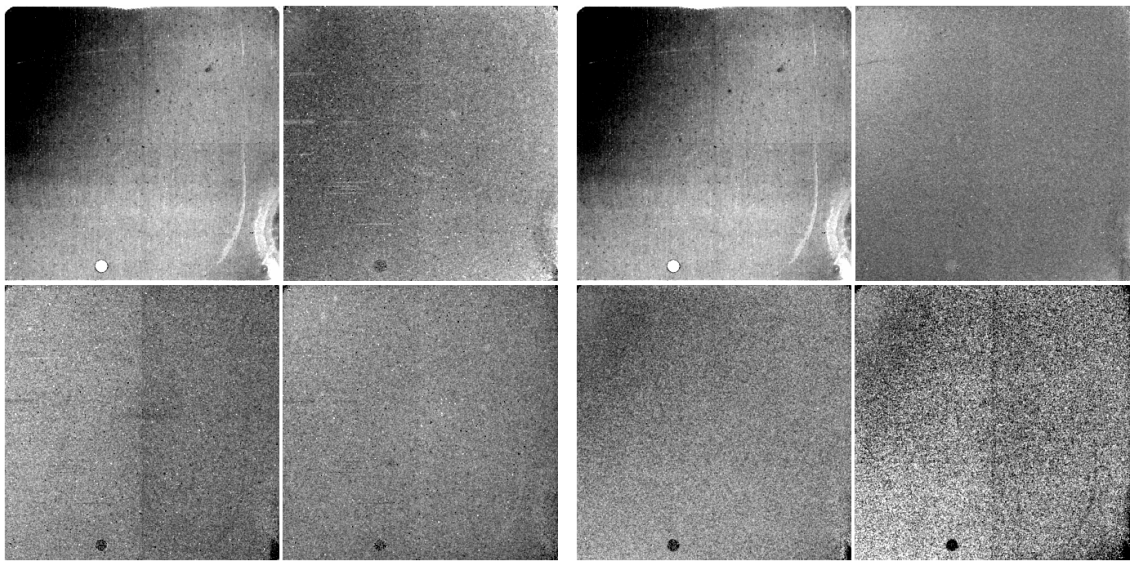

Figure 9. Two comparisons of correction flats constructed from 3 identical visits consisting of a 303 s tungsten exposure followed by a series of darks. The upper left hand image in both panels is the correction flat constructed from all three visits scaled from 0.8 to 1.2. In the left hand panel, the other three images are the difference between a correction flat constructed with just one visit and the flat constructed from all three visits. These difference images are scaled from -0.1 to 0.1. As elsewhere, the frames are presented with an inverted greyscale, so the upper right image in the left hand panel shows that a correction flat constructed from this visit has more persistence in quadrants 1 and 2 than the flat constructed from all three visits. In the right hand panel, the other three images are flats constructed with darks obtained from 0 - 2000 s after the tungsten exposure (upper right), 2000 - 4000 s (lower left) and 4000 - 6000 s (lower right). All of the images have been smoothed slightly.

the detector than others, and this would cause differences in the persistence flat generated from darks obtained with small and large time delays. We know that persistence varies with both exposure time and saturation level. Therefore correction flats generated from darks obtained after short tungsten lamp exposures might be different from those obtained after long exposures. Similarly, for the same tungsten lamp exposure times, flats generated from visits with a narrow band tungsten exposure (low fluence level) are likely to be different from those generated after a wide band tungsten exposure (high fluence level). A complete investigation of these variations are beyond the scope of the available data. Nevertheless, we can explore some of the possibilities.

Of the 47 visits used to generate the correction flat, there are three nominally identical visits in program ID 12351 – 17, 27 and A7 – with tungsten lamp exposures through the F105W filter of 303 s, which resulted in a stimulus images with average exposure levels of about 210,000 e, or about 3 times saturation. The correction flats produced from the darks in all 3 visits, and the difference between the individual correction flats and the average flat, are shown in the left hand panel of Fig. 9. The standard deviation of the difference between the correction flats based on each of the individual visits and the correction flat based on the average of the 3 visits is about 3%. The standard deviation between the flat derived from these three visits and the flat produced using all 47 visits is about 2%. For each of the visits, darks were obtained over a period of about 6000 seconds after the initial tungsten exposure. A comparison of correction flats obtained using darks from the entire interval to that using data from 0 - 2000 s, 2000 - 4000 s and 4000 - 6000s after the initial tungsten exposure is shown in the right hand panel of Fig. 9. The standard deviation of smoothed versions these flats to the average flat was 2%, 3% and 6% respectively for each time interval. Some trends are also apparent, particularly with respect to the amount of excess persistence in quadrant 1.

Evaluation of the improvement when the correction flat is used

In order to evaluate whether the correction flat represents a substantial improvement to the persistence model, we have applied the persistence model to all of the data obtained in Cycle 21, program 13572, with and without the correction flat. These span a large range of exposure times. This is the same program from which the coefficients for the so-called power law model were developed.

We have then determined the average error in persistence in each of the darks, and in each of the four quadrants of the detector. The errors as a function of time after the stimulus image are shown in Fig. 10 for pixels with a stimulus between 1×10^5 and 5×10^6 e. The upper panels in the figure show the results without a correction flat; the lower panels show results with the correction flat. The panels on the left hand side include the errors that are contained in the spatially-averaged model; the panels on the right hand side show the results with the mean error in persistence removed. The overall shape of the various panels, with larger errors at short delay times, is simply due to the fact that persistence itself is decaying with time. It is clear from comparing the top and bottom panels in the figure that including a correction flat reduces the errors in the

model.

Spatial variations in persistence and other properties of the detector

Persistence is not the only property of the IR detector on WFC3 that exhibits spatial variations. Other characteristics that vary spatially include the well-depth, the quantum efficiency, and the dark current.

As noted earlier, persistence is thought to be associated with traps in the detector diodes. The shape of the WFC3 detector's persistence curve, and in particular the rapid rise in persistence amplitude between a fluence of about 30,000 and 100,000 e, indicates that the density of these traps increases near saturation. Different pixels in the detector have different saturation levels, and so one might expect, given uniform illumination, that persistence would be greatest in regions with the smallest saturation levels. The upper right image in Fig. 11 shows a smoothed version of the saturation thresholds as a function of position in the detector as derived by Hilbert (2014). The large-scale pattern of the persistence variations (upper left image in Fig. 11) does not resemble that expected if the saturation threshold were correlated with persistence. If it were, we would expect high persistence in Quadrant 2. Note though that one of the two small "blotches" of higher persistence in the upper right quadrant shows a low saturation level. However, there are other low saturation regions such as the long thin arc as well as the wagon wheel in the lower right quadrant, which correlate not with higher but with lower persistence.

A flat field (the so-called p- or pixel flat) is applied to the data to correct for sensitivity variations across the field of view; the flat fielding step in the calibration pipeline also applies the gain conversion, converting pixels from instrumental values of DN to electrons. Although the flat in principle corrects for a variety of effects in the WFC3 IR channel, the primary calibration is for quantum efficiency variations within the detector. The raw data are divided by the pflat so regions where the flat is high represent regions of higher than normal quantum efficiency. As shown in the lower left image in Fig. 11, with the exception of the handful of obvious extended artifacts (e.g. death star, wagon wheel, debonded pixels) and some very small-scale features, the pflat is relatively flat across the field of view. Interestingly, the pipeline flat shows no significant change in the upper left corner (where the persistence map is highest), just a modest (few percent) high region near the top center region of the detector. On smaller scales, some features show contradictory behavior which is not fully understood. For example, the long narrow arc in the lower right quadrant shows up with low persistence correction and low saturation levels yet high values in the flat field while portions of the wagon wheel are low in all three regimes: persistence, saturation, and pipeline flat. The feather-shaped artifact in the pipeline flat, extending upward from the lower right quadrant, does not appear at all in either the persistence correction or in the saturation map while the long linear feature running through the upper right quadrant in the pipeline flat is discernible as low in the saturation map but invisible in the persistence correction flat.

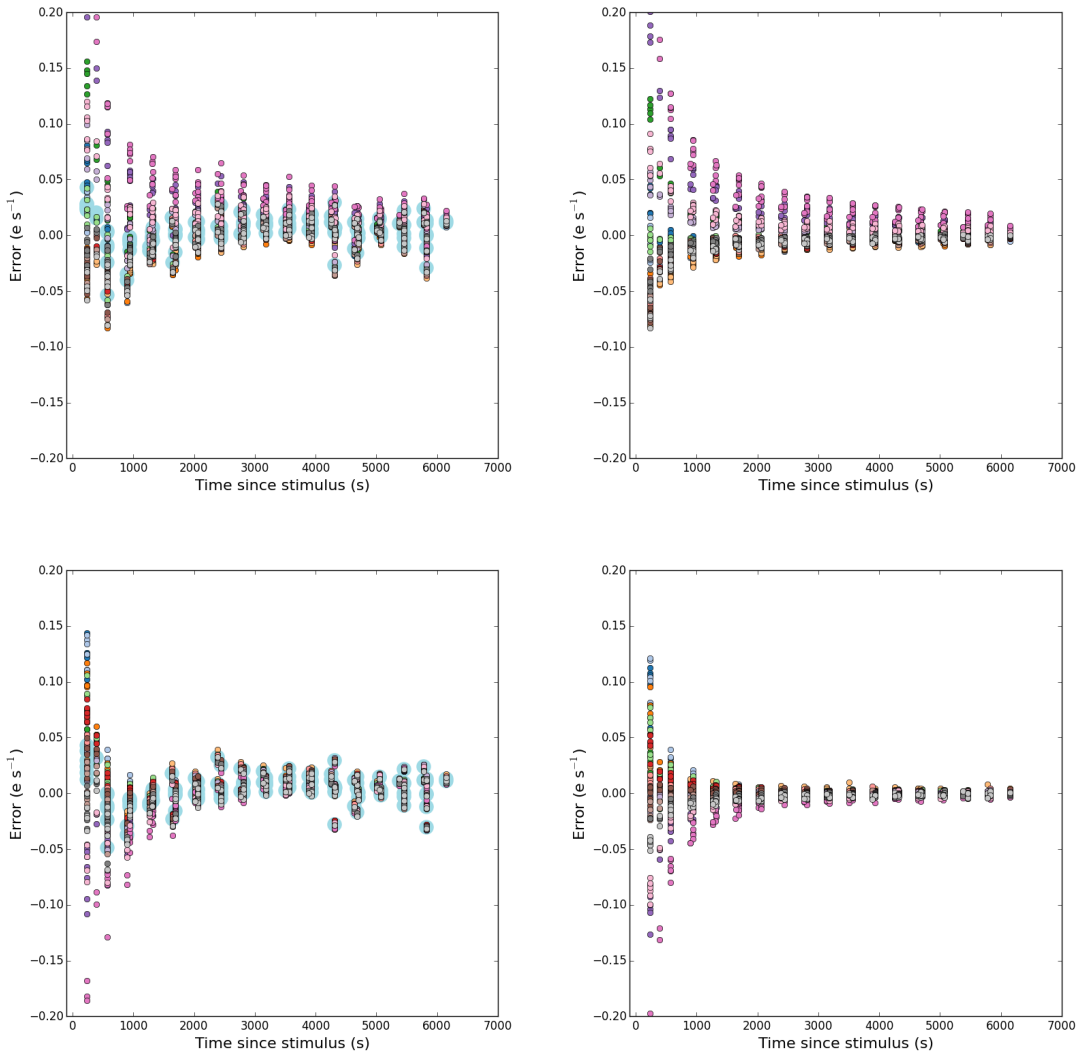

Figure 10. Top: The errors in the persistence calculated for the average persistence model without the application of the correction flat. The left panel shows the average error (pale blue filled circles) for each dark and the errors in 16 (4x4) sections of the detector (small dots of various colors). The right hand panel shows the errors if the average error is removed. Bottom: Same as top except the correction flat has been applied.

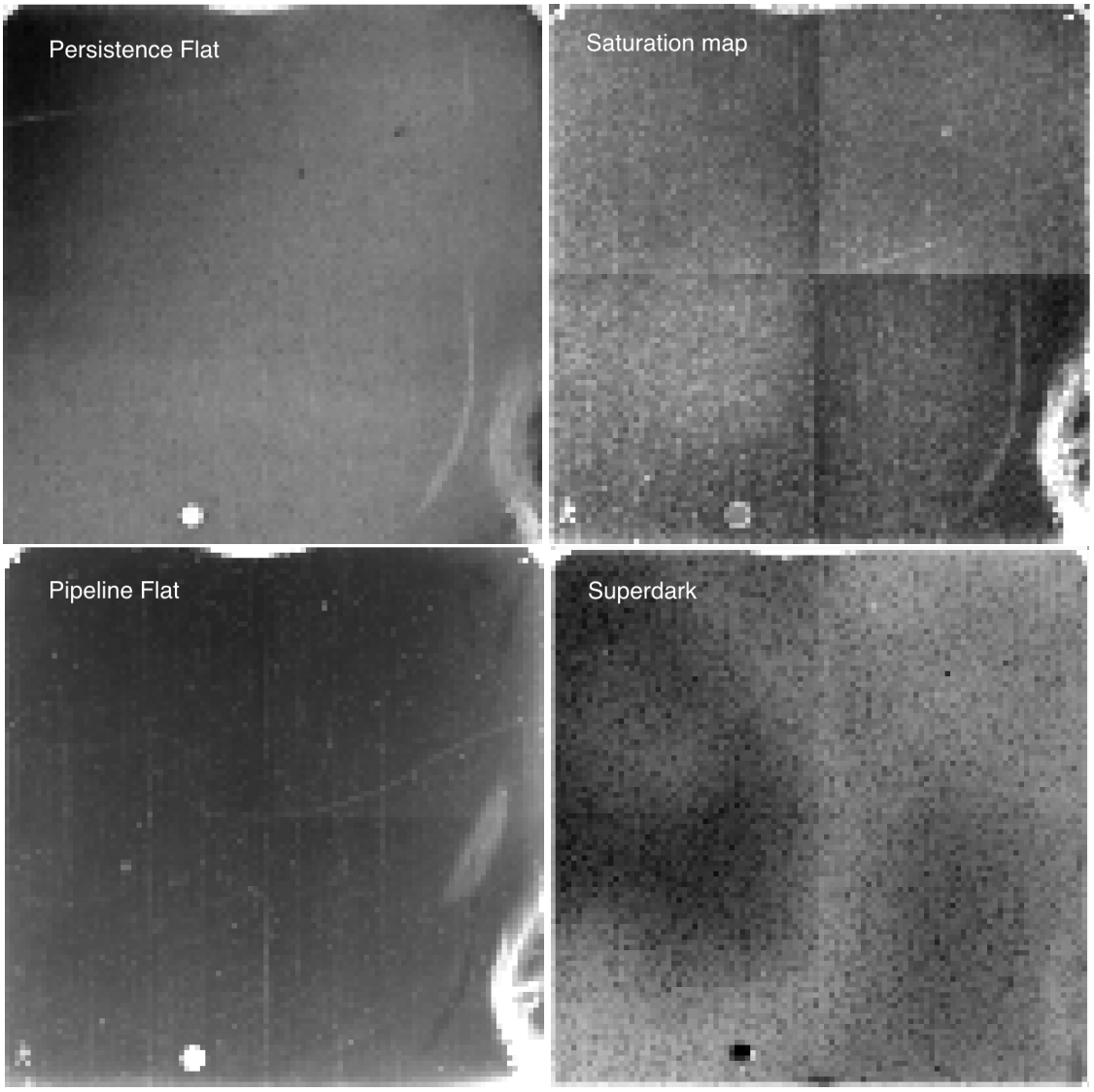

Figure 11. Clockwise from upper left is a persistence correction flat, the saturation map, the normalized superdark and the pipeline flatfield. All images have been smoothed via 10x10 block-averaging and are shown with inverted greyscales. Levels, clockwise from upper left, are 0.5-1.5, 30000-35000 DN, 0.5-1.5, and 0.8-1.2.

A superdark is applied to the data during calibration in order to remove the signature of the dark current. Using the long spars200 pipeline superdark (x5g1509ki_drk.fits, exptime 2800 sec), which is constructed from a stack of 44 input dark ramps, we compare the spatial pattern in the dark to that of the persistence flat. To improve the visibility of any large-scale pattern which might be present, first the hot pixels flagged in the image fits file data quality extension and their adjacent pixels (upper, lower, right, and left) are replaced with the median value of the good pixels. The resulting "clean" superdark as well as the persistence correction flat are then block-averaged using 10x10 pixel regions and are shown in Fig. 11. The correction flat is highest in the upper left corner while the highest pixel values in the superdark occur primarily in a donut-shaped region straddling the left two quadrants. The correction flat has the lowest values mainly in the lower right quadrant while the superdark has its lowest pixel values at the lower edge of the lower left quadrant and in the upper right corner. There does not appear to be any correlation of the large-scale persistence correction flat pattern with the superdark pattern; in fact, the superdark pattern is more similar to the saturation map (pixels with lower saturation levels have higher dark current). On a small scale, we note that one of the two small blotches of higher persistence in the upper right quadrant (originally identified and circled in green in Fig. 5) shows a higher dark level as well as a lower saturation threshold.

Summary and Conclusions

Here, we have made the first systematic attempt to investigate spatial variations in persistence in the WFC3 IR detector. There are clear variations in persistence across the detector, with the most pronounced persistence in the outer corner of quadrant 1. The variations appear primarily on large spatial scales; pixel to pixel variations are small. Overall, the variations do not seem to be directly associated with variations in the saturation levels, quantum efficiency, or dark current.

We have characterized the spatial variation in persistence in WFC3 in terms of a correction to the spatially-averaged model. We have shown that using a correction flat, derived from a series of visits comprised of tungsten exposures followed by darks, provides a significant improvement in the persistence correction (e.g. factor of 2 reduction in errors, peak to peak, at 2000 s), at least on the datasets described here. The correction flat is incorporated into the persistence prediction software used to estimate persistence in HST images and available through MAST (Version 3.0.1 of the persistence software). To the extent that persistence variations are simply amplitude variations, it should be possible to improve the persistence predictions with a more targeted set of visits consisting of tungsten flats followed by darks, and a follow-up program to do just this has been approved for Cycle 23 (Prog. ID 14380).

Given the various demands on HST time, it will be more difficult to completely characterize variations in the decay time for persistence, i.e. the power law decay exponent γ, as a function of position. A program to develop such a model requires visits comprised of external exposures of a dense star field because they provide a much wider

range of saturation level in each region of the detector than does a visit that begins with a tungsten lamp exposure. Ideally, one would like enough data to accurately measure persistence in of order 10 x 10 regions of the detector. A more modest program has been approved for Cycle 23 (Prog. ID 14381). It should provide enough data to accurately measure persistence in at least 16 (4 x 4) regions on the detector for four different exposure times. This should allow us to develope the first complete spatially-dependent model of persistence in the WFC3 IR detector, and to determine whether additional observations would significantly improve the model.

Acknowledgments

We thank George Chapman, Merle Reinhart, Alan Welty, and Bill Januszewski for their help in crafting and executing this program and Gabriel Brammer for a careful reading of this manuscript.

References

Hilbert, B & Petro L., 2012, "WFC3/IR Dark Current Stability," WFC3 ISR 2012-11

Hilbert, B. 2014, "Updated non-linearity calibration method for WFC3/IR," WFC3 ISR 2014-17

Long, K. S., Baggett S. M., & MacKenty, J. W. , 2013a, "Characterizing Persistence in the WFC3 IR Channel: Finite Trapping Times," WFC3 ISR 2013-06

Long, K. S., Baggett S. M., & MacKenty, J. W. , 2013b, "Characterizing Persistence in the WFC3 IR Channel: Observations of Omega Cen", WFC3 ISR 2013-07

Long, K. S., Baggett S. M., & MacKenty, J. W. , 2015, "Persistence in the WFC3 IR Detector: An Improved Model Incorporating the Effects of Exposure Time", WFC3 ISR 2015-15

Long, K.S., Baggett, S.M., MacKenty, J.W., and Riess, A.G., 2012, "Characterizing persistence in the IR detector within the Wide Field Camera 3 instrument on the Hubble Space Telescope," Proceedings of the SPIE, 8442, 84421W-9

Smith, R.M., Zavodny, M., Rahmer, G. & Bonati, M., 2008a, "A theory for image persistence in HgCdTe photodiodes," Proceedings of the SPIE, 7021, 70210J-1

Smith, R. M., Zavodny, M., Rahmer, G., Bonati, M., 2008b, "Calibration of image persistence in HgCdTe photodiodes," Proceedings of the SPIE, 7021, 70210K-1